

Supporting information

Tuning electron transfer in supramolecular nano-architectures made of fullerenes and porphyrins

Bingzhe Wang,^a Stefan Bauroth,^{a,c} Avishek Saha,^a Muqing Chen,^{d*} Timothy Clark,^{c*} Xing Lu,^{b*} Dirk M. Guldi^{a*}

^aDepartment of Chemistry and Pharmacy & Interdisciplinary Center for Molecular Materials, Friedrich-Alexander-Universität Erlangen-Nürnberg, Egerlandstrasse 3, 91058 Erlangen, Germany,

^bState Key Laboratory of Materials Processing, School of Material Science and Engineering, Huazhong University of Science and Technology, 1037 Luoyu Road, 430074 Wuhan, China.

^cComputer-Chemie-Centrum, Department of Chemistry and Pharmacy, Friedrich-Alexander-Universität Erlangen-Nürnberg, Nägelsbachstrasse 25, 91052 Erlangen, Germany

^dDepartment of Materials Science and Engineering, University of Science and Technology of China, 230026 Hefei, China

Contents

1. General Experimental Section	3
2. Synthesis.....	5
2.1 Synthesis of C₆₀-Pyr, C₆₀-Ar-Pyr and C₆₀-(Ar)₂-Pyr	5
2.2 Synthesis of ZnP-TDP	7
3. Photophysical characterization.....	8
3.1 Photophysical characterization of C₆₀-Pyr, C₆₀-Ar-Pyr, C₆₀-(Ar)₂-Pyr and ZnP-TDP	8
3.1.1 Absorption and emission	8
3.1.2 Transient absorption	10
3.1.3 Spectroelectrochemistry	14
3.2 Photophysical characterization of the complexes.....	15
3.2.1 Absorption and emission	15
3.2.2 Transient absorption	17
3.2.3 Energy level diagram	25
4. Calculation.....	26

1. General Experimental Section

NMR spectroscopy

¹H NMR spectra were referenced to TMS at 7.26 ppm, while ¹³C NMR spectra were referenced to residual CHCl₃ at 77.16 ppm.

Mass spectrometry

Matrix-assisted laser desorption-ionization time-of flight (MALDI-TOF) mass spectra were recorded with a Biflex III (Bruker Daltonics Inc., Germany) mass spectrometer using 1,1,4,4-tetraphenyl-1,3-butadiene as matrix in a positive ion linear mode.

Electrochemistry

Electrochemical data were obtained by cyclic voltammetry using a conventional single-compartment three-electrode cell arrangement in combination with a potentiostat "AUTOLAB®, eco chemie". As the auxiliary and reference electrodes, Pt and Ag wires were used, respectively, while the working electrode was a glassy carbon electrode. Tetrabutylammonium hexafluorophosphate (TBAPF₆ = 0.1 M) was used as a supporting electrolyte at room temperature. All potentials are referenced to ferrocene/ferrocenium.

UV/vis absorption spectroscopy

Steady state absorption spectra were obtained using a Perkin Elmer Lambda 2 UV/vis two-beam spectrophotometer with a slit width of 2 nm and a scan rate of 480 nm min⁻¹. A quartz glass cuvette of 10 × 10 mm was used.

Emission spectroscopy

Steady state emission was recorded using a Horiba Jobin Yvon FluoroMax-3 spectrometer with a slit width of 2 nm for excitation and emission and an integration time of 0.2 s. A quartz glass cuvette of 10 × 10 mm was used. All spectra were corrected for the instrument response. For excitation wavelength below 450 nm a cut off filter (435 nm) was inserted.

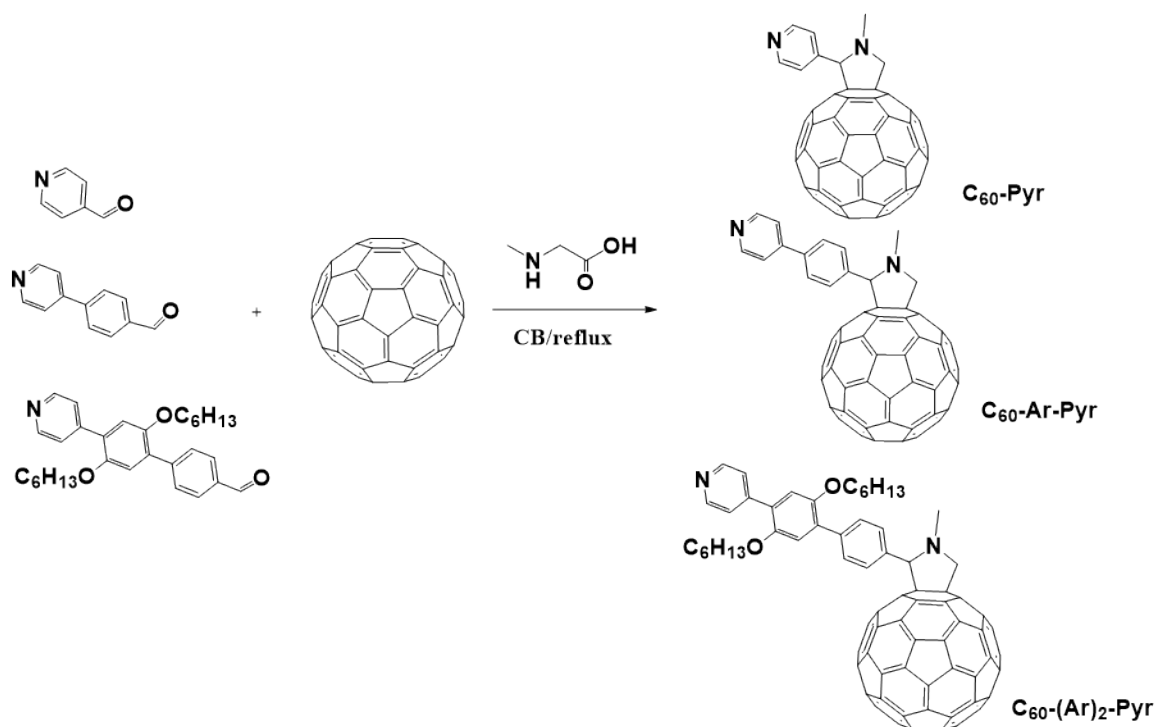
Fs-transient absorption spectroscopy

Femtosecond transient absorption studies were performed with laser pulses (1 kHz, 150 fs pulse width) by using an amplified Ti/sapphire laser system (Model CPA 2110, Clark-MXR Inc.; output 775 nm). For an excitation wavelength of 430 nm, a nonlinear optical parametric converter (NOPA) was used to generate ultra-short tunable visible pulses out of the pump pulses. The transient absorption pump probe spectrometer (TAPPS) is a two-beam setup, in which the pump pulse is used as the excitation source for transient species and the delay of the probe pulse is exactly controlled by an optical delay rail. As the probe (white-light

continuum), a small fraction of pulses stemming from the CPA laser system were focused by a 50 mm lens into a 2 mm thick sapphire disc. The transient spectra were recorded using fresh argon-saturated solutions in each laser excitation. All experiments were performed in a 2 mm quartz cuvette.

2. Synthesis

2.1 Synthesis of C_{60} -Pyr, C_{60} -Ar-Pyr and C_{60} -(Ar)₂-Pyr



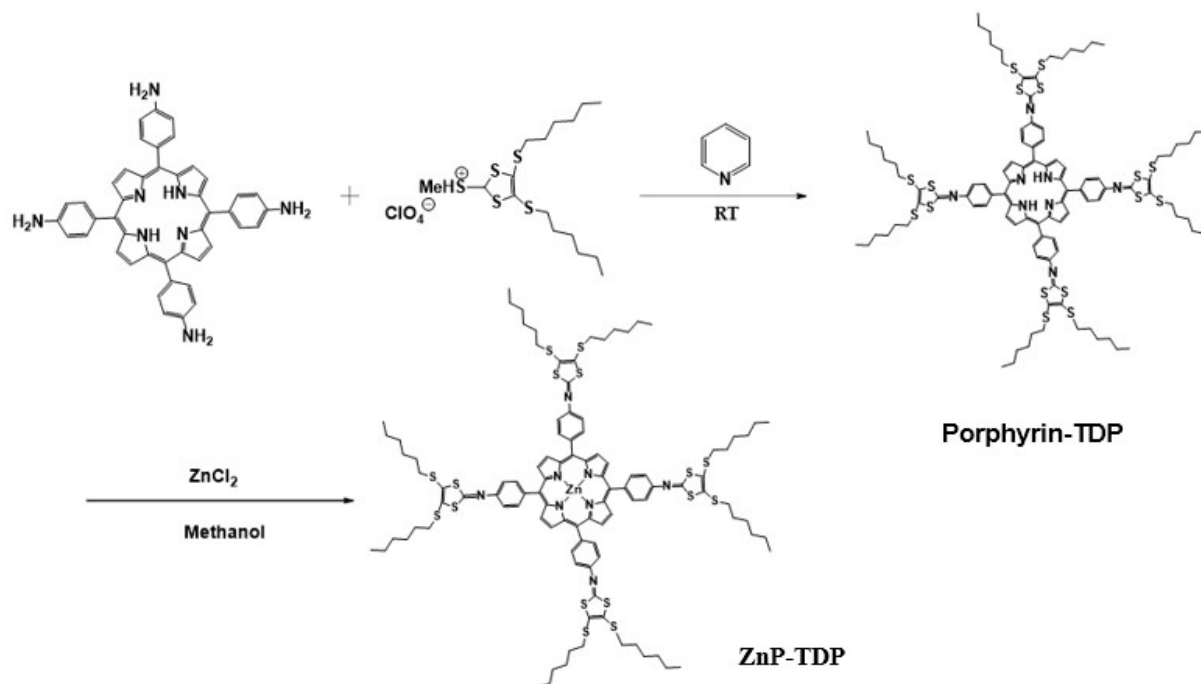
To synthesis C_{60} -Pyr, fullerene C_{60} (0.68g, 0.94mmol) was added to the chlorobenzene solution of isonicotinaldehyde (0.1g, 0.94 mmol) and sarcosine (0.11 g, 1.88mmol). The mixed solution was refluxed under the argon atmosphere and the reaction process was monitored by TLC technology. When the reaction finished, the chlorobenzene solvent was removed by reduced pressure and the residual solid was purified by flash column chromatography on silica gel (200-300 mesh, toluene), affording the brown solid product (0.3g) with the yield of 37%. ¹H NMR (600 MHz, CDCl₃/CS₂) δ 8.66 (d, J = 4.4 Hz, 2H), 7.72 (s, 2H), 5.03 (d, J = 9.3 Hz, 1H), 4.95 (s, 1H), 4.33 (d, J = 9.3 Hz, 1H), 2.87 (s, 3H). ¹³C NMR (151 MHz, CDCl₃/CS₂) δ 155.67, 153.49, 152.51, 152.01, 150.39, 147.39, 147.38, 146.42, 146.39, 146.34, 146.31, 146.28, 146.26, 146.21, 146.06, 146.05, 145.75, 145.72, 145.70, 145.66, 145.51, 145.43, 145.34, 145.32, 145.31, 145.30, 144.79, 144.68, 144.48, 144.41, 143.26, 143.15, 142.83, 142.76, 142.73, 142.70, 142.32, 142.27, 142.25, 142.24, 142.17, 142.15, 142.08, 142.05, 141.98, 141.90, 141.80, 141.69, 140.40, 140.15, 139.69, 137.15, 136.49, 136.11, 135.69, 128.44, 123.99, 82.49, 76.49, 70.16, 69.06, 40.12. MALDI-TOF MS, experimental molecular weight is 854.61, and corresponding theoretical value is 855.09.

The reaction of C_{60} -Ar-Pyr and C_{60} -(Ar)₂-Pyr are similar to that of C_{60} -Pyr. For C_{60} -Ar-Pyr, the crude product was purified by flash column chromatography (eluent: CS₂/ethyl acetate=8/1), affording 335 mg C_{60} -Ar-Pyr with the yield of 23%. ¹H NMR (600 MHz, CDCl₃/CS₂) δ 8.62 (dd, J = 4.6, 1.5 Hz, 2H), 7.94 (s, 2H), 7.73 (d, J = 8.3 Hz, 2H), 7.49 (dd, J = 4.6, 1.5 Hz, 2H), 5.03 (t, J = 4.5 Hz, 2H), 4.33 (d, J = 9.3 Hz, 1H), 2.88 (s, 3H). ¹³C NMR (151 MHz, CDCl₃/CS₂) δ 156.04, 153.80, 153.12, 152.84, 150.44, 147.36, 147.19, 146.60, 146.42, 146.40, 146.36, 146.30, 146.28, 146.22, 146.19, 146.09, 146.03, 145.78, 145.72, 145.67, 145.54, 145.50, 145.41, 145.40, 145.34, 145.31, 145.25, 144.80, 144.66, 144.49, 144.42, 143.26, 143.14, 142.81, 142.74, 142.71, 142.68, 142.34, 142.32, 142.26, 142.24, 142.15, 142.14, 142.05, 141.97, 141.91, 141.80, 141.66, 140.37, 140.35, 140.11, 139.69, 138.45, 138.18, 137.10, 136.58, 136.03, 135.77, 121.37, 83.28, 77.09, 70.18, 69.04, 40.18. MALDI-TOF MS, experimental molecular weight is 930.84, and

corresponding theoretical value is 931.12.

For **C₆₀-(Ar)₂-Pyr**, the crude product was purified by flash column chromatography (eluent: CS₂/ethyl acetate=12/1), affording 370 mg **C₆₀-(Ar)₂-Pyr** with the yield of 64%. ¹H NMR (600 MHz, CDCl₃/CS₂) δ 8.63 (d, *J* = 4.0 Hz, 2H), 7.86 (s, 2H), 7.62 (dd, *J* = 38.1, 6.3 Hz, 4H), 7.02 (s, 1H), 6.96 (s, 1H), 5.01 (d, *J* = 11.8 Hz, 2H), 4.30 (d, *J* = 9.3 Hz, 1H), 3.96 (t, *J* = 6.4 Hz, 2H), 3.81 (t, *J* = 6.4 Hz, 2H), 2.87 (s, 3H), 1.69 (dd, *J* = 14.4, 6.8 Hz, 2H), 1.55 (dd, *J* = 14.1, 6.8 Hz, 2H), 1.42 – 1.33 (m, 2H), 1.23 (ddd, *J* = 16.1, 13.3, 5.1 Hz, 10H), 0.85 (dt, *J* = 10.6, 7.0 Hz, 6H). ¹³C NMR (151 MHz, CDCl₃/CS₂) δ 156.26, 154.04, 153.44, 153.42, 150.55, 150.46, 148.85, 147.33, 147.31, 146.84, 146.64, 146.50, 146.34, 146.31, 146.25, 146.23, 146.15, 146.13, 145.97, 145.79, 145.63, 145.57, 145.55, 145.48, 145.42, 145.34, 145.31, 145.27, 145.25, 145.18, 144.76, 144.61, 144.44, 144.40, 143.19, 143.06, 142.73, 142.64, 142.62, 142.31, 142.29, 142.20, 142.19, 142.14, 142.11, 142.08, 141.98, 141.83, 141.74, 141.57, 140.27, 140.22, 139.94, 139.49, 138.13, 136.91, 136.60, 135.97, 135.80, 132.28, 127.27, 124.38, 115.89, 115.71, 83.47, 70.15, 69.71, 69.50, 69.09, 40.15, 31.70, 31.66, 29.49, 26.00, 25.91, 22.93, 22.83, 14.36, 14.21. MALDI-OF MS, experimental molecular weight is 1208.11, and corresponding calculation value is 1208.33.

2.2 Synthesis of **ZnP-TDP**



A mixture of (4,5-bis(hexylthio)-1,3-dithiol-2-yl)(methyl)sulfonium perchlorate (2.3 g, 4.76 mmol), 4,4',4'',4'''-(5H,10H,15H,20H,22H,24H-porphyrin-5,10,15,20-tetra-yl)tetraaniline (0.8 g, 1.19 mmol) were dissolved in pyridine (25 ml) and stirred at room temperature for 12 h. After finishing this reaction, the pyridine solvent was removed by reduced pressure and the residual solid was purified by silicon column chromatography three times, affording the purple product tetrakis(4-((1,3-dithiol-2-ylidene)methyl)phenyl)porphyrin (**Porphyrin-TDP**) with yield of 21%. 1H NMR (600 MHz, $CDCl_3$) δ 8.96 (s, 8H), 8.26 (d, $J = 7.5$ Hz, 8H), 7.46 (d, $J = 8.0$ Hz, 8H), 2.98 (t, $J = 7.3$ Hz, 8H), 2.92 (t, $J = 7.4$ Hz, 8H), 1.76 (ddd, $J = 31.5, 15.0, 7.4$ Hz, 16H), 1.54 – 1.47 (m, 16H), 1.38 (d, $J = 20.4$ Hz, 32H), 0.97 (t, $J = 5.7$ Hz, 12H), 0.93 (s, 12H), -2.69 (s, 2H). ^{13}C NMR (151 MHz, $CDCl_3$) δ 167.73, 164.61, 150.13, 138.89, 135.81, 132.32, 130.92, 128.85, 127.84, 125.41, 119.79, 118.57, 65.58, 36.49, 36.45, 31.38, 29.87, 29.66, 28.33, 28.24, 22.60, 22.57, 14.08. MALDI-OF MS, experiment weight is 2007.18; the corresponding calculation weight is 2007.22. The obtained porphyrin-TFF later dissolved in methanol, and the $ZnCl_2$ was added in the solution. After stirred at 60°C and 8h, the solvent was removed. The residual solid was purified using silicon column chromatography, affording a purple-black solid **ZnP-TDP** with yield of 67%. 1H NMR (600 MHz, Acetone- d_6) δ 9.05 (s, 8H), 8.16 (d, $J = 5.5$ Hz, 8H), 7.60 – 7.50 (m, 2H), 7.35 (ddd, $J = 8.6, 5.3, 2.9$ Hz, 1H), 6.58 (s, 5H), 2.90 (t, $J = 6.4$ Hz, 8H), 2.57 (s, 8H), 1.70 (s, 8H), 1.59 – 1.12 (m, 58H), 0.99 (s, 12H), 0.86 (s, 12H). ^{13}C NMR (151 MHz, $CDCl_3$) δ 150.24, 140.35, 135.34, 131.11, 130.30, 128.00, 124.95, 121.78, 120.33, 117.78, 36.26, 36.09, 31.36, 31.12, 29.70, 29.31, 28.26, 27.92, 22.61, 22.40, 14.11, 13.99. MALDI-OF MS, experiment weight is 2069.68; the corresponding calculation weight is 2069.51.

3. Photophysical characterization

3.1 Photophysical characterization of C_{60} -Pyr, C_{60} -Ar-Pyr, C_{60} -(Ar)₂-Pyr and ZnP-TDP

3.1.1 Absorption and emission

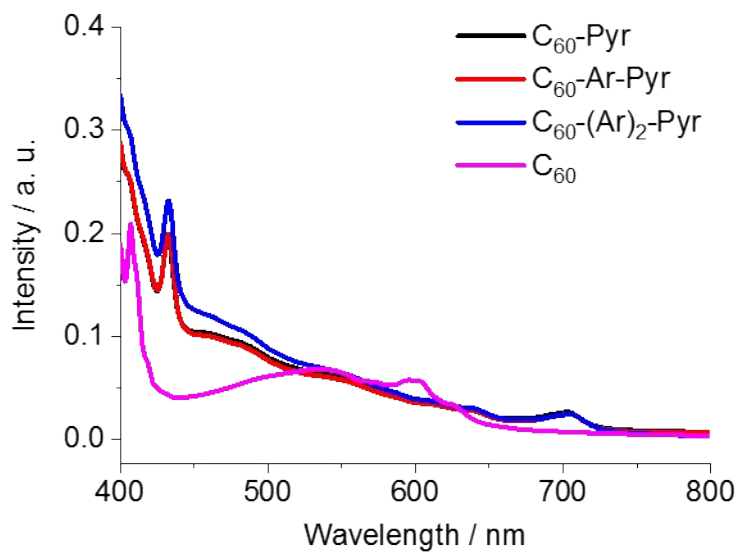


Figure S1 Room temperature absorption spectra of 0.5×10^{-5} M C_{60} -Pyr (black), C_{60} -Ar-Pyr (red), C_{60} -(Ar)₂-Pyr (blue) and C_{60} (pink) in chlorobenzene.

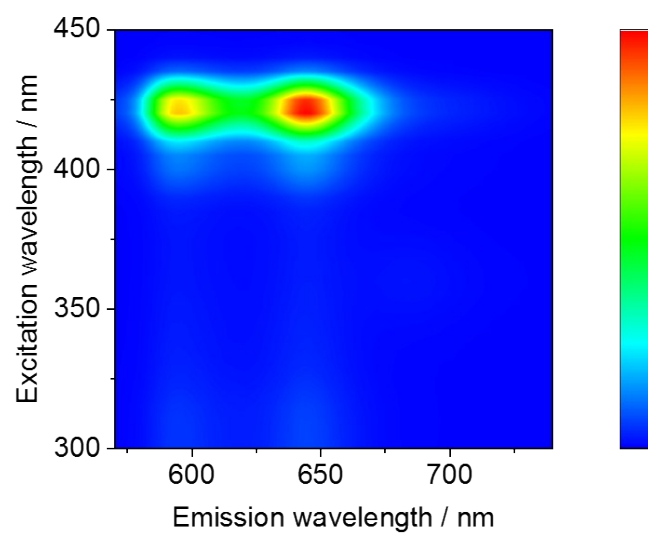


Figure S2 3D fluorescence mapping of **ZnP** upon different excitation wavelength from 300 to 450 nm. The scale bar from black to red is 0 to 2.5×10^7 .

3.1.2 Transient absorption

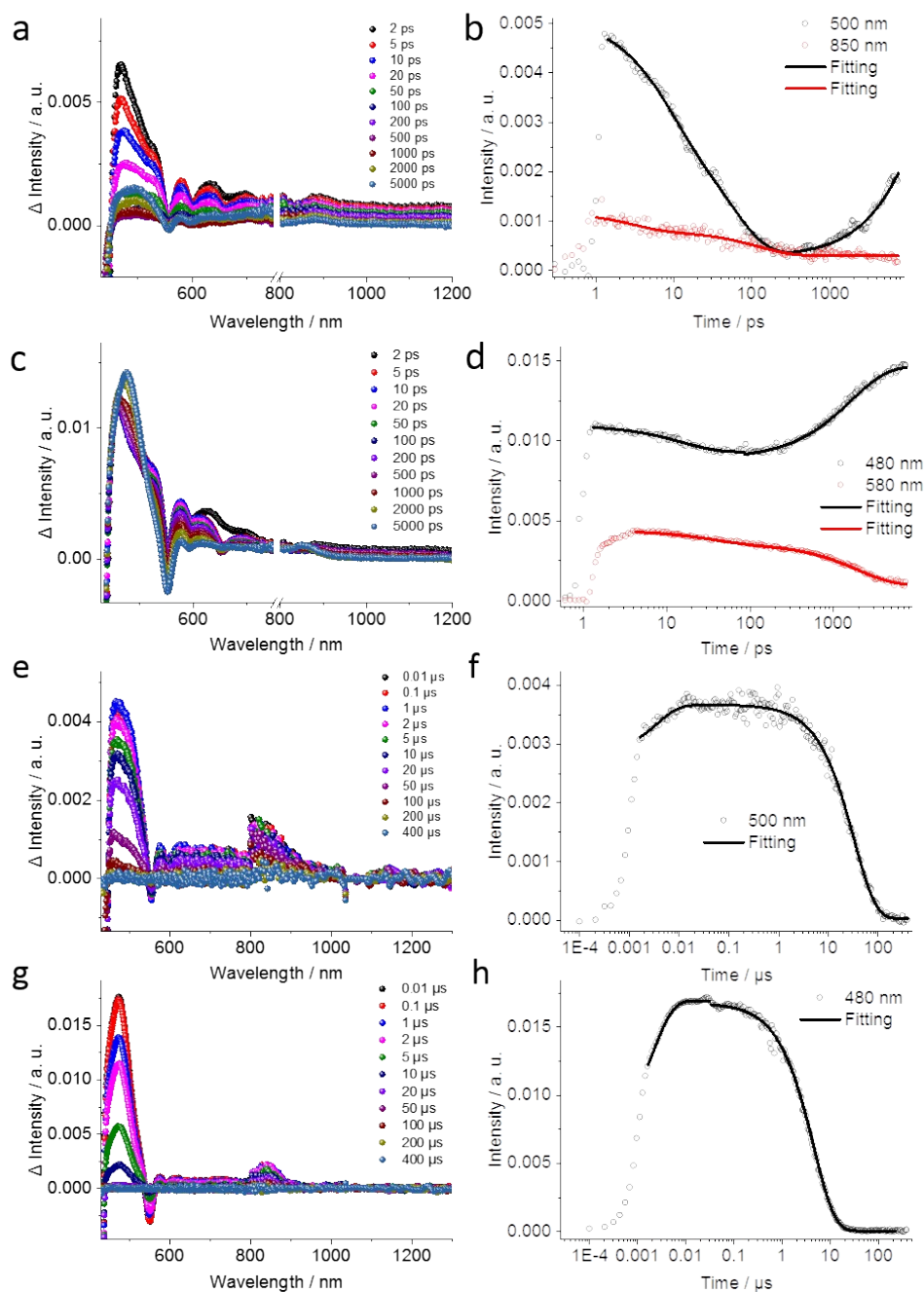


Figure S3 Differential absorption spectra obtained upon femtosecond pump probe experiments at room temperature (430 nm and 500 nJ) of (a) **ZnP-TDP** and (c) **ZnP** in chlorobenzene with time delays between 2 and 5000 ps – for time delays see Figure legend. (b, d) show the time-absorption profiles of the spectra shown at 500 and 850 nm to demonstrate the intersystem crossing process. Differential absorption spectra obtained upon nanosecond pump probe experiments at room temperature (430 nm and 500 nJ) of (e) **ZnP-TDP** and (g) **ZnP** in chlorobenzene with time delays between 0.01 to 400 μ s – for time delays see Figure legend. (f, h) show the time-absorption profiles of the spectra shown at 500 nm to demonstrate the triplet excited state decays.

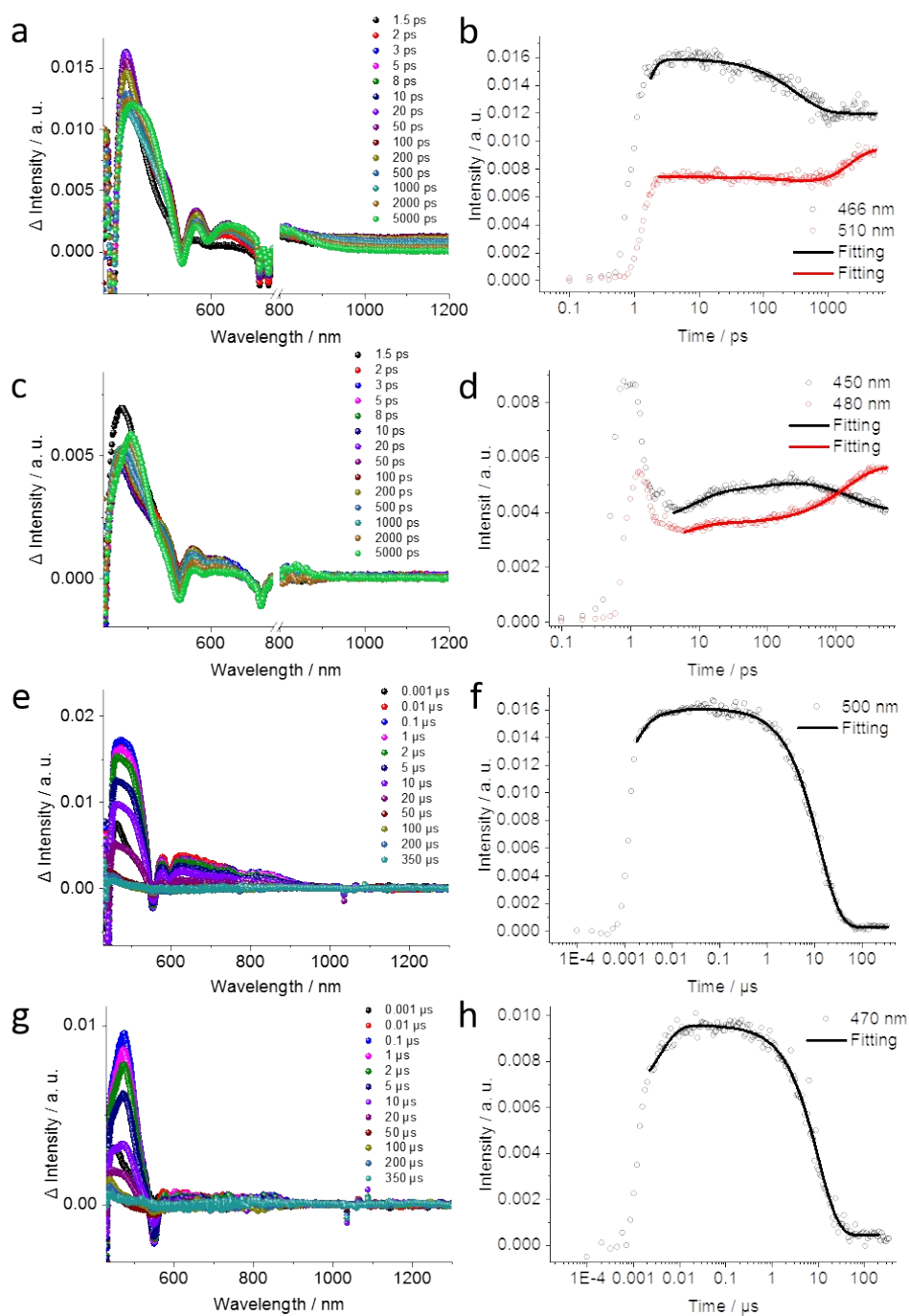


Figure S4 Differential absorption spectra obtained upon femtosecond pump probe experiments at room temperature (320 nm and 500 nJ) of (a) **ZnP-TDP** and (c) **ZnP** in chlorobenzene with time delays between 1.5 and 5000 ps – for time delays see Figure legend. (b,d) show the time-absorption profiles of the spectra shown at 460 and 500 nm to demonstrate the intersystem crossing process. Differential absorption spectra obtained upon nanosecond pump probe experiments at room temperature (320 nm and 500 nJ) of (e) **ZnP-TDP** and (g) **ZnP** in chlorobenzene with time delays between 0.001 to 350 μ s – for time delays see Figure legend. (f, h) show the time-absorption profiles of the spectra shown at 500 nm to demonstrate the triplet excited state decays.

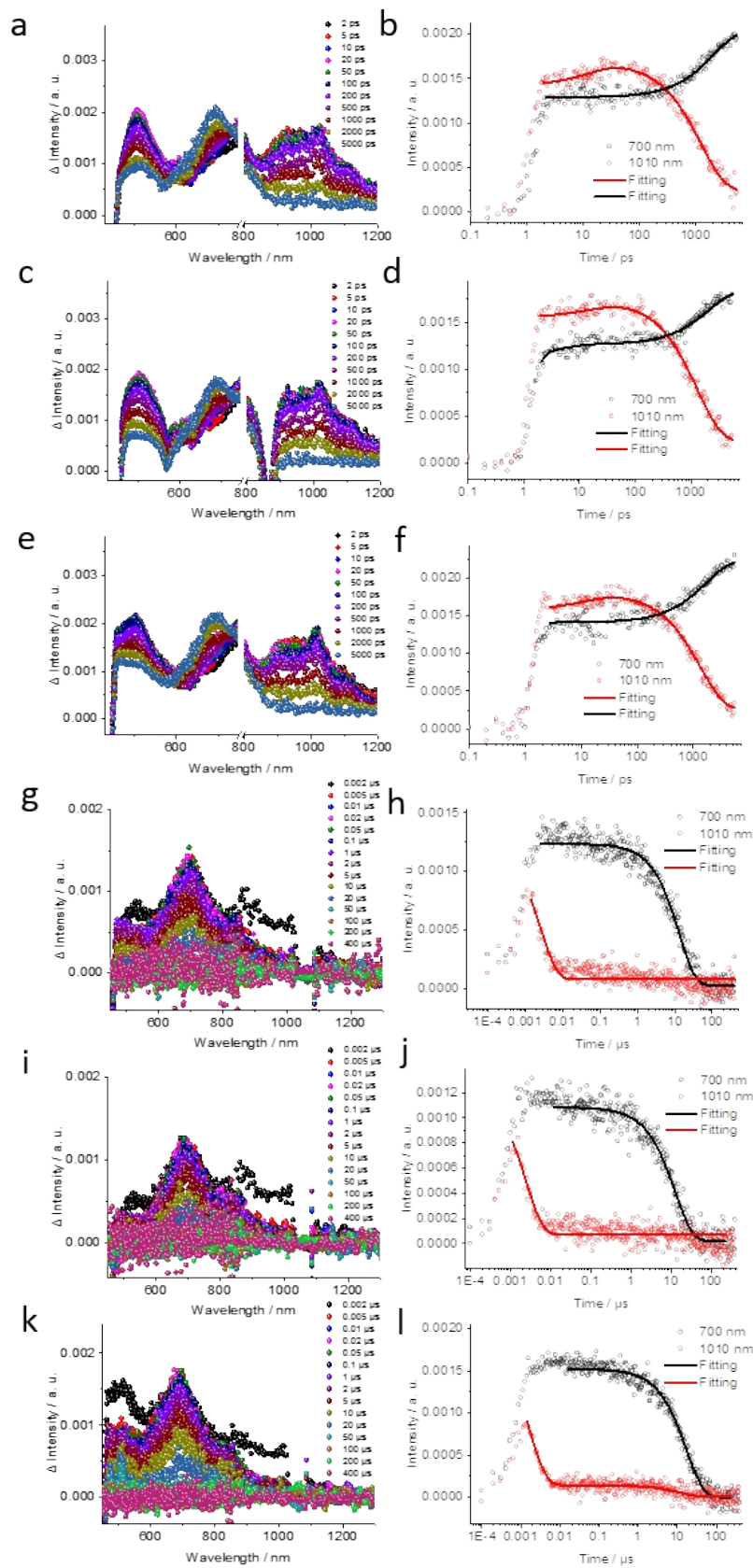


Figure S5 Differential absorption spectra obtained upon femtosecond pump probe experiments at room temperature (430 nm and 500 nJ) of 2×10^{-4} M (a) **C₆₀-Pyr**, (c) **C₆₀-Ar-Pyr** and (e) **C₆₀-(Ar)₂-Pyr** in chlorobenzene with time delays between 2 and 5000 ps – for time delays see Figure legend. (b, d, f) show the time-absorption profiles of the spectra shown at 700 and 1010 nm to demonstrate the intersystem crossing process.

Differential absorption spectra obtained upon nanosecond pump probe experiments at room temperature (430 nm and 500 nJ) of 2×10^{-4} M (g) **C₆₀-Pyr**, (i) **C₆₀-Ar-Pyr** and (k) **C₆₀-(Ar)₂-Pyr** in chlorobenzene with time delays between 0.01 to 400 μ s – for time delays see Figure legend. (h, j, l) show the time-absorption profiles of the spectra shown at 700 and 1010 nm to demonstrate the singlet and triplet excited state decays.

Table S6 Singlet and triplet excited state lifetimes of **ZnP-TDP**, **ZnP**, **C₆₀-Pyr**, **C₆₀-Ar-Pyr** and **C₆₀-(Ar)₂-Pyr** in chlorobenzene at room temperature obtained from exponential fittings of the time profiles upon femtosecond / nanosecond pump probe experiments (430 nm and 500 nJ).

Compound	S1 \longrightarrow T1	T1 \longrightarrow S0
ZnP-TTF	3.68 \pm 0.54 ns	34.43 \pm 0.90 μ s
ZnP	1.94 \pm 0.03 ns	4.49 \pm 0.05 μ s
C₆₀-Pyr	2.03 \pm 0.10 ns	12.26 \pm 0.90 μ s
C₆₀-Ar-Pyr	1.92 \pm 0.06 ns	16.04 \pm 0.37 μ s
C₆₀-(Ar)₂-Pyr	1.84 \pm 0.14 ns	15.35 \pm 0.22 μ s

3.1.3 Spectroelectrochemistry

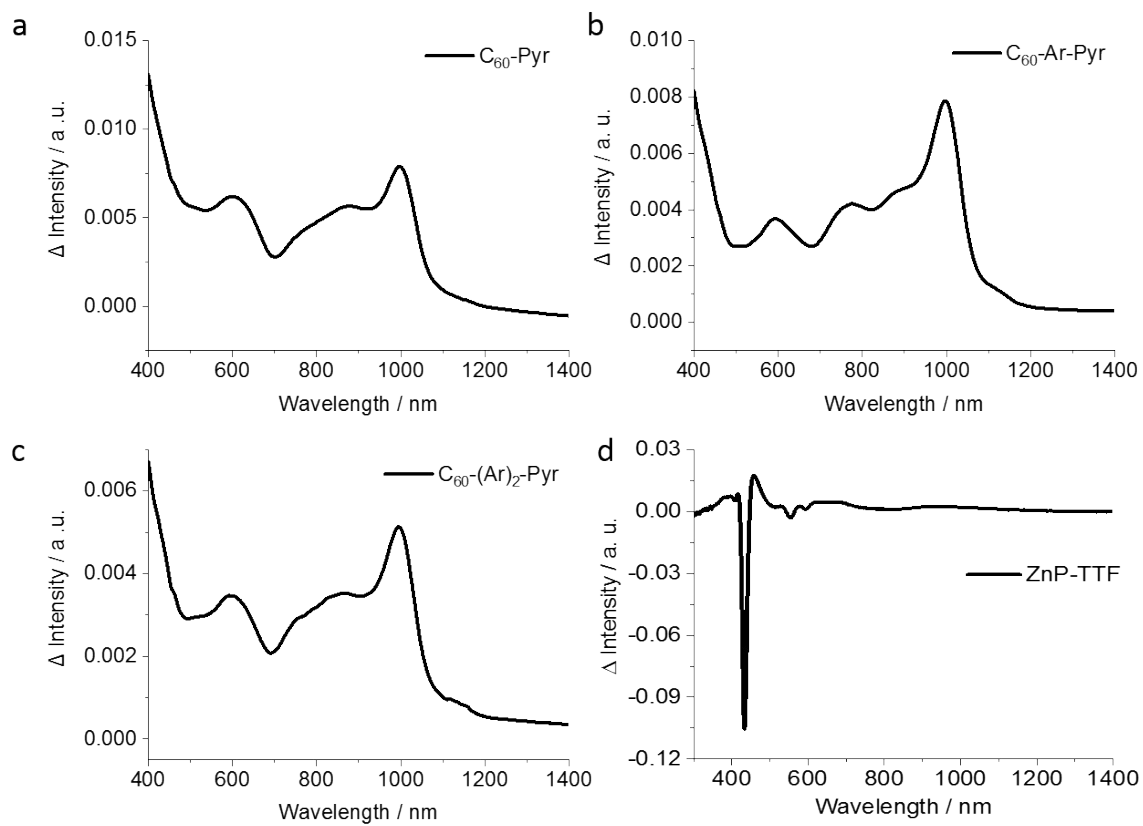


Figure S7 Differential absorption spectrum (visible and near-infrared) obtained upon electrochemical reduction of (a) C₆₀-Pyr, (b) C₆₀-Ar-Pyr·ZnP-TDP and (c) C₆₀-(Ar)₂-Pyr·ZnP-TDP with an applied potential of -0.7 V and oxidation of (d) ZnP-TDP under 0.8 V in chlorobenzene with 0.1 M TBAPF₆ vs. Ag-wire.

3.2 Photophysical characterization of the complexes

3.2.1 Absorption and emission

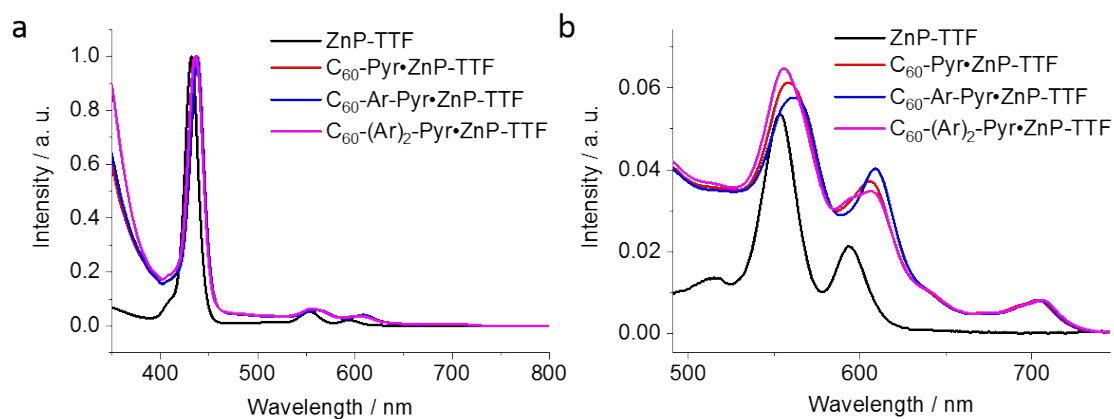


Figure S8 Normalized room temperature (a) absorption spectra in toluene of 0.5×10^{-5} M **ZnP-TDP** (black) with 1×10^{-4} M **C₆₀-Pyr** (Red), **C₆₀-Ar-Pyr** (blue) and **C₆₀-(Ar)₂-Pyr** (pink). (b) shows the zoom in on the absorption features of the Q-bands.

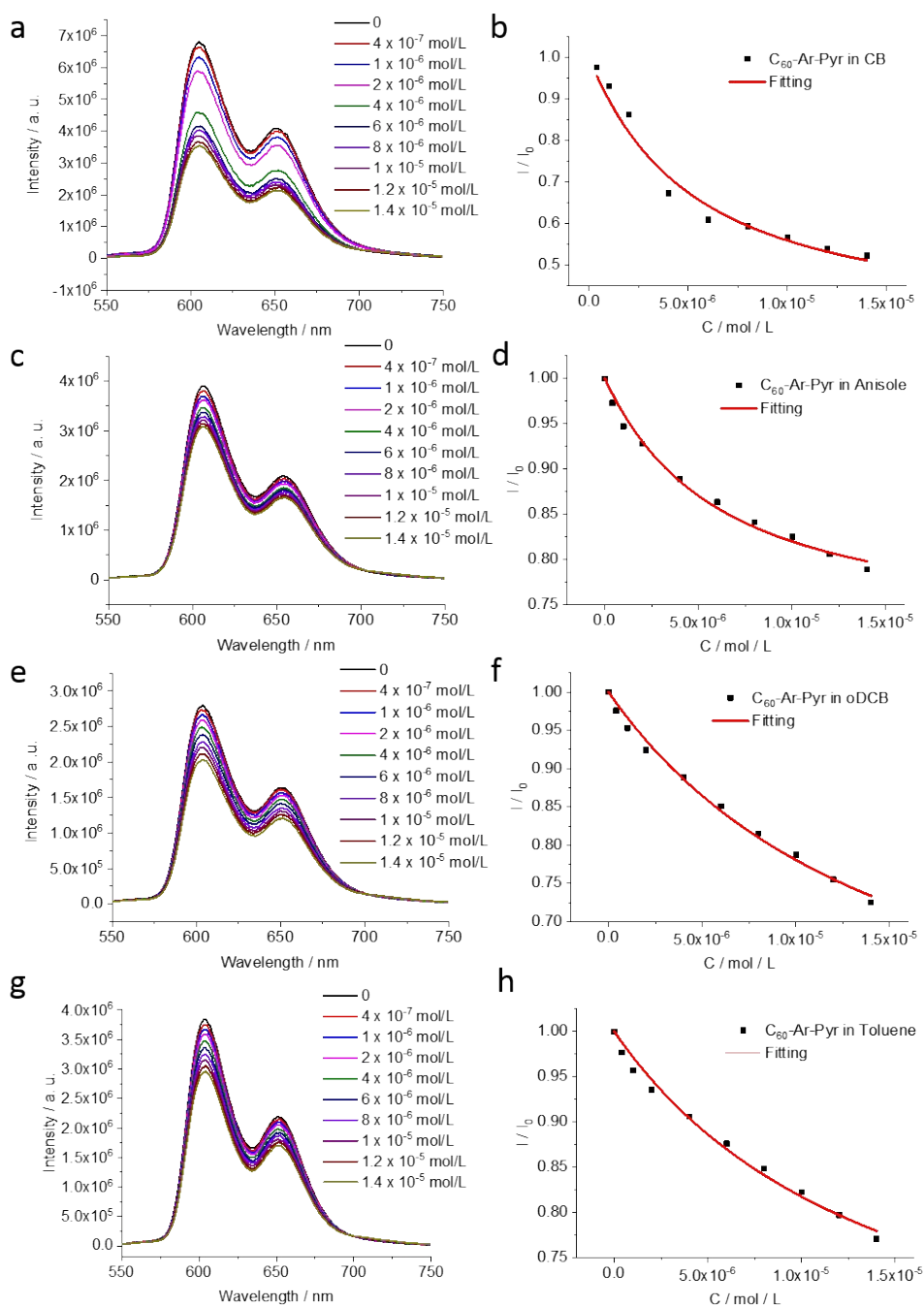


Figure S9 Emission changes observed during the complexation of **ZnP-TDP** (4×10^{-8} M) upon addition of **C₆₀-Ar-Pyr** ($0 - 1.4 \times 10^{-5}$ M) excited at 430 nm in (a) chlorobenzene, (c) anisole, (e) oDCB and (g) toluene. (b,d,f,h) shows the changes of intensity and the fits.

3.2.2 Transient absorption

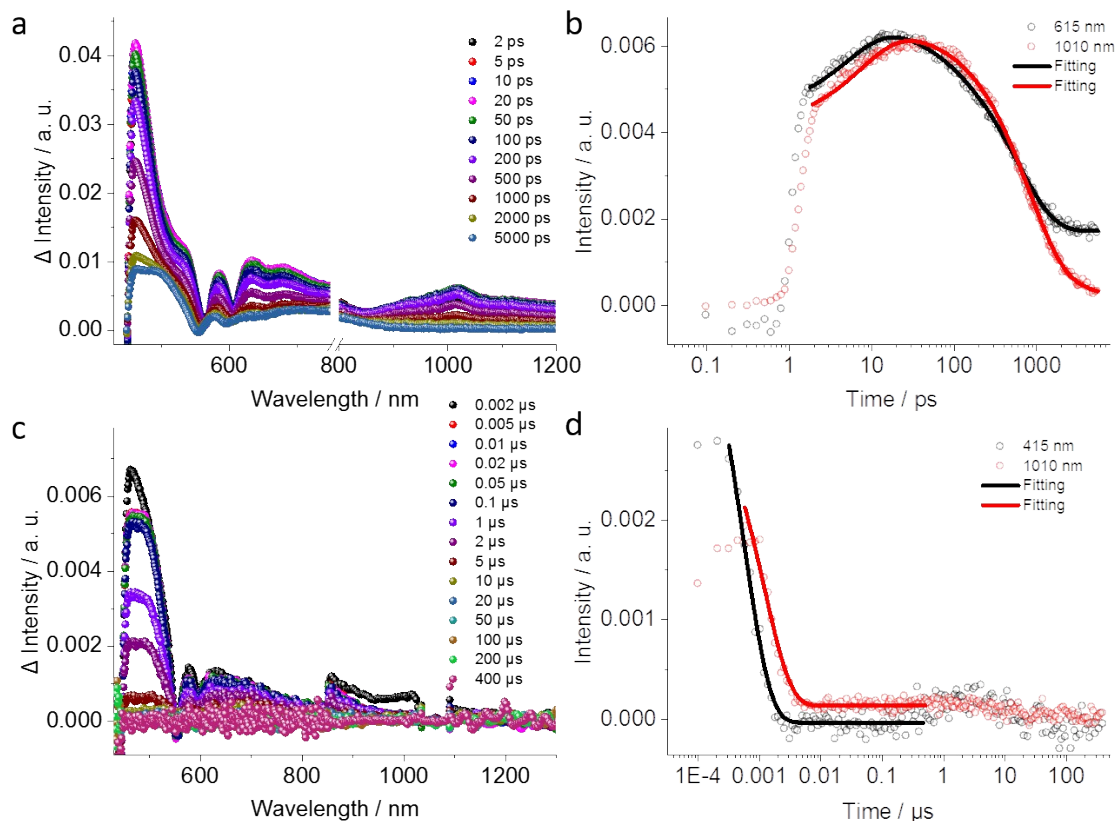


Figure S10 Differential absorption spectra obtained upon femtosecond pump probe experiments (430 nm and 500 nJ) of C_{60} -Pyr·ZnP-TDP in chlorobenzene with time delays between 2 and 5000 ps (a) and 0.002 to 400 μ s (c) at room temperature. (b) shows the time-absorption profiles of the spectra at 615 and 1010 nm to demonstrate the charge separation process and (d) shows the time-absorption profiles of the spectra at 415 and 1010 nm to demonstrate the charge recombination process.

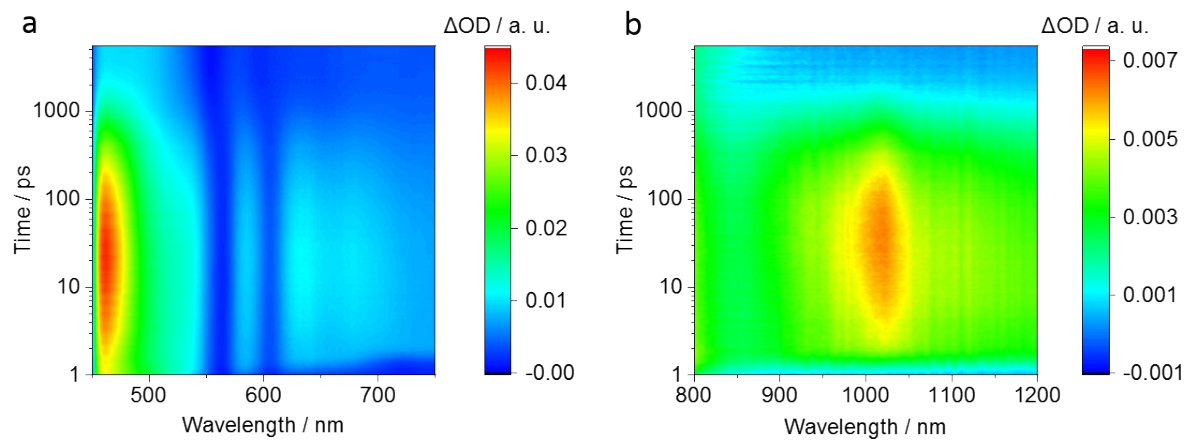


Figure S11 Differential absorption changes in (a) the visible and in (b) the near-infrared obtained upon femtosecond pump-probe experiments (430 nm / 500 nJ) of C_{60} -Pyr·ZnP-TDP in chlorobenzene at room temperature.

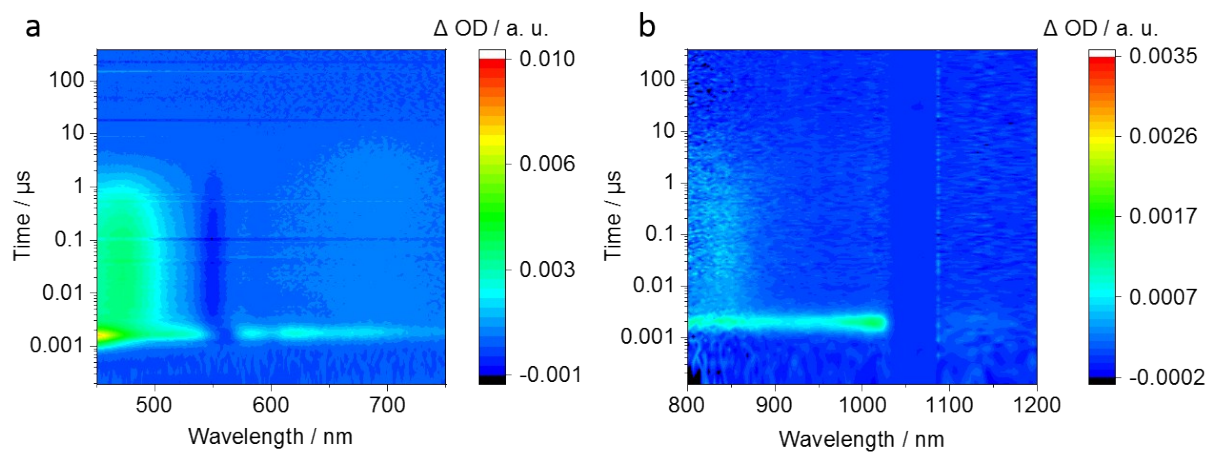


Figure S12 Differential absorption changes in (a) the visible and in (b) the near-infrared obtained upon nanosecond pump-probe experiments (430 nm / 500 nJ) of **C₆₀-Ar-Pyr·ZnP-TDP** in chlorobenzene at room temperature.

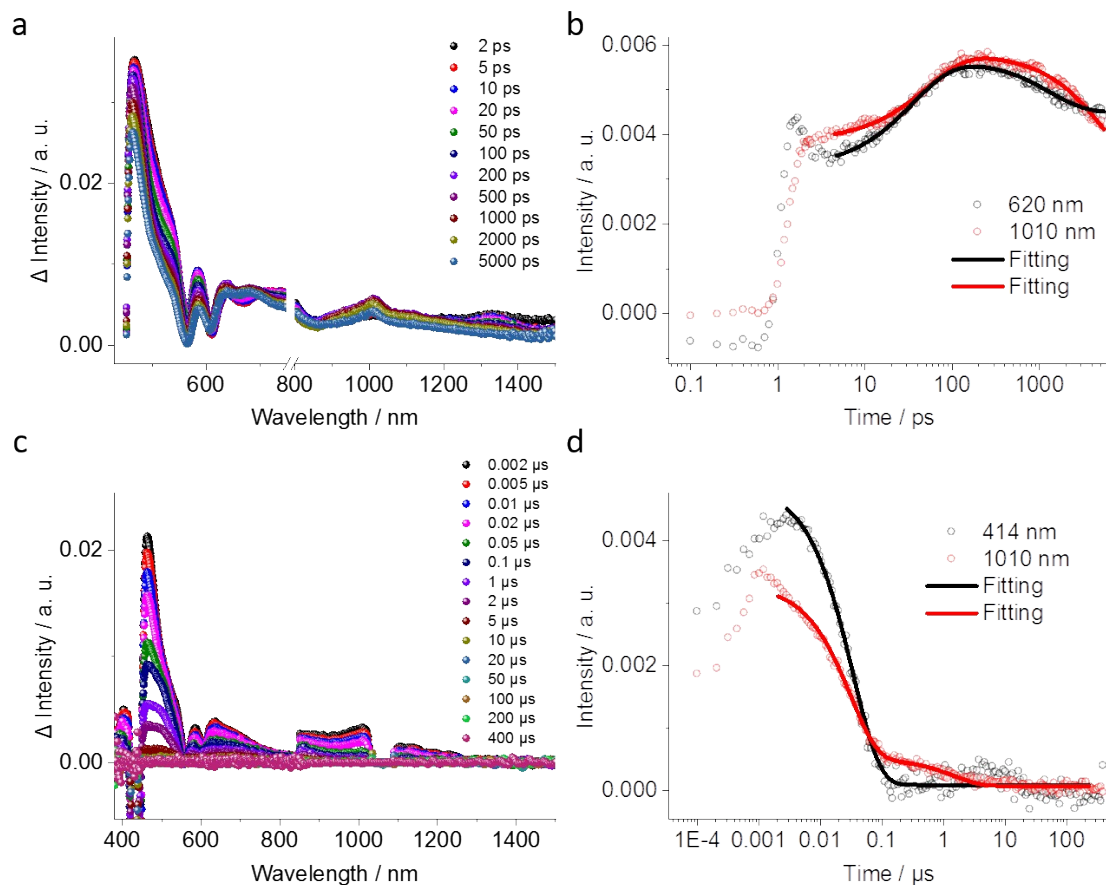


Figure S13 Differential absorption spectra obtained upon femtosecond pump probe experiments (430 nm and 500 nJ) of C_{60} -Ar-Pyr·ZnP-TDP in chlorobenzene with time delays between 2 and 5000 ps (a) and 0.002 to 400 μ s (c) at room temperature. (b) shows the time-absorption profiles of the spectra at 615 and 1010 nm to demonstrate the charge separation process and (d) shows the time-absorption profiles of the spectra at 415 and 1010 nm to demonstrate the charge recombination process.

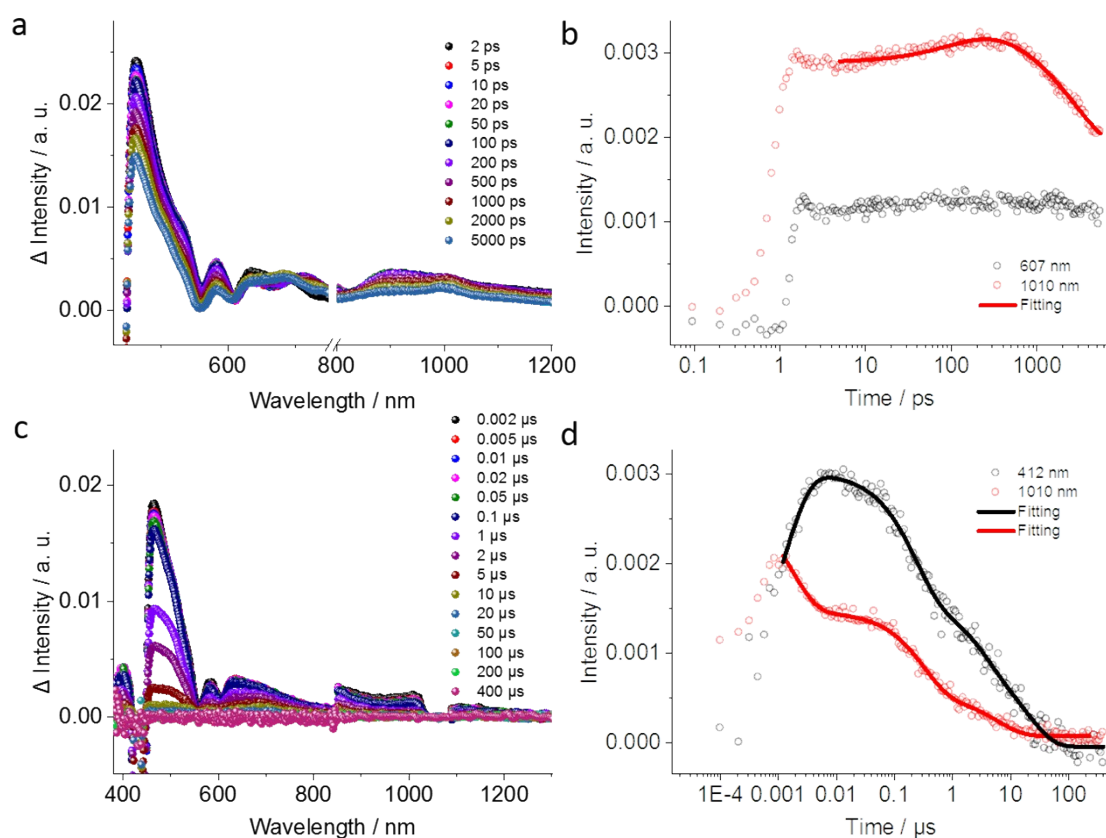


Figure S14 Differential absorption spectra obtained upon femtosecond pump probe experiments (430 nm and 500 nJ) of $C_{60}-(Ar)_2-Pyr \cdot ZnP-TDP$ in chlorobenzene with time delays between 2 and 5000 ps (a) and 0.002 to 400 μ s (c) at room temperature. (b) shows the time-absorption profiles of the spectra at 607 and 1010 nm to demonstrate the charge separation process and (d) shows the time-absorption profiles of the spectra at 412 and 1010 nm to demonstrate the charge recombination process.

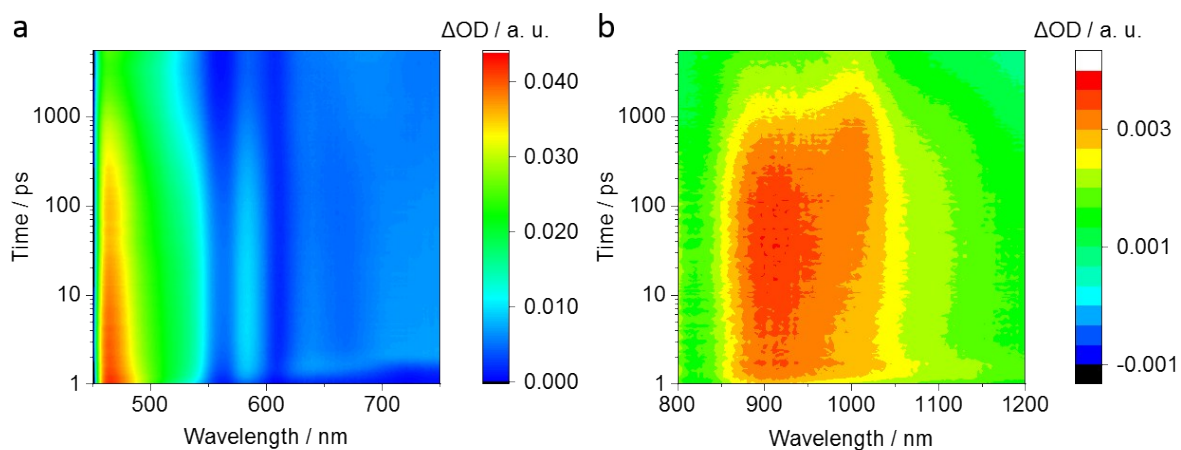


Figure S15 Differential absorption changes in (a) the visible and in (b) the near-infrared obtained upon femtosecond pump-probe experiments (430 nm / 500 nJ) of $C_{60}-(Ar)_2-Pyr \cdot ZnP-TDP$ in chlorobenzene at room temperature.

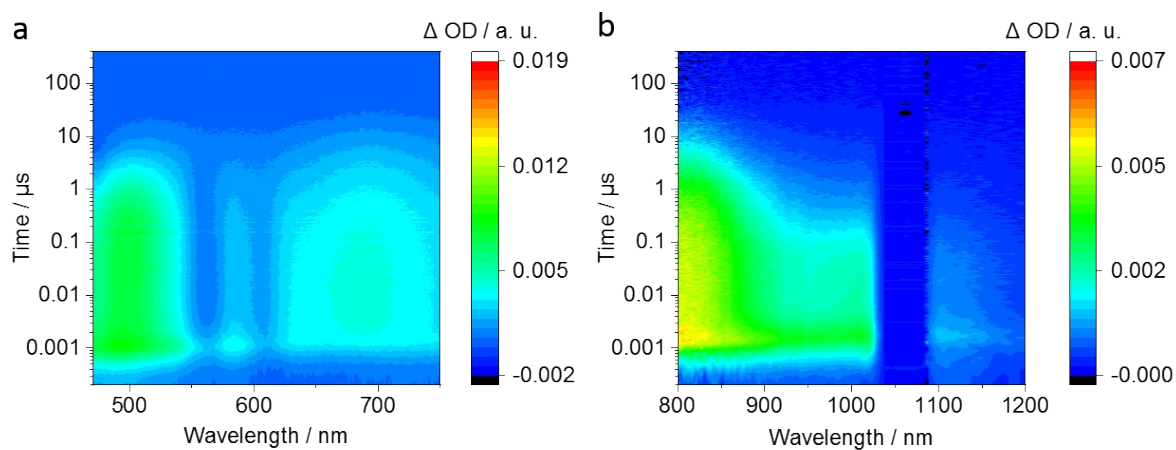


Figure S16 Differential absorption changes in (a) the visible and in (b) the near-infrared obtained upon nanosecond pump-probe experiments (430 nm / 500 nJ) of **C₆₀-Ar-Pyr·ZnP-TDP** in chlorobenzene at room temperature.

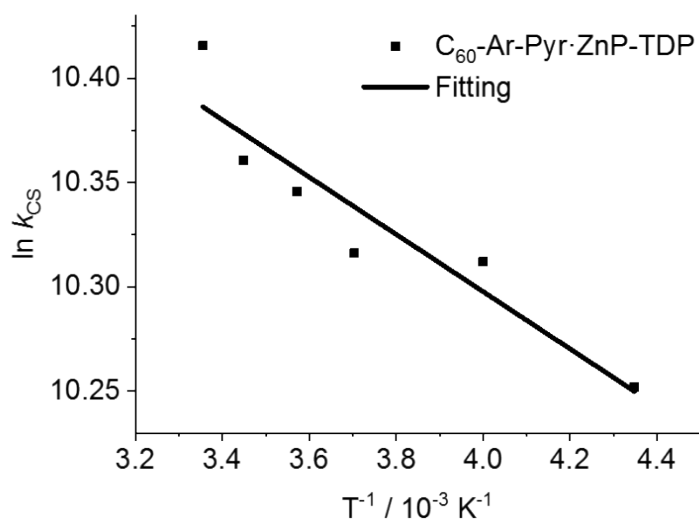


Figure S17 Plot of $\ln k_{CS}$ versus $1/T$ for $C_{60}\text{-Ar-Pyr-ZnP-TDP}$. The lines are fitted in the linearized form. The CS rates are obtained through differential absorption measurements upon femtosecond pump probe experiments (430 nm and 500 nJ) in chlorobenzene.

3.2.3 Energy level diagram

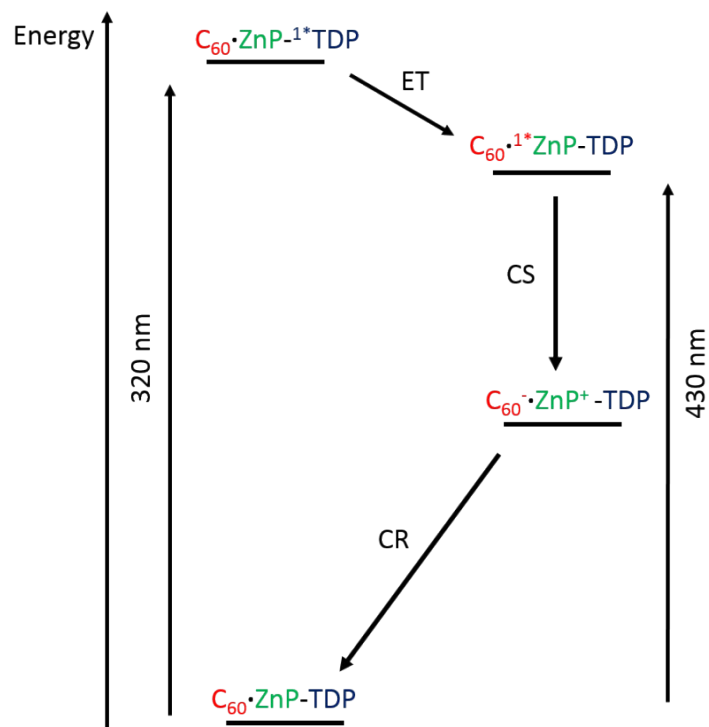


Figure S18 Energy level diagram for the complexes, ET: energy transfer, CS: charge separation, CR: charge recombination.

4. Calculation

Computational results obtained using software programs from Dassault Systèmes BIOVIA. Forcefield calculations were performed with the Forcite program, and graphical displays generated with BIOVIA Materials Studio.

Preoptimizations are performed with a modified Dreiding forcefield. As the original Dreiding forcefield only includes zinc in tetragonal binding fashion, the square planar Zn-N bond in porphyrins was parametrized with respect to B3LYP/def2TZVP optimizations. Similar the axial coordination of a pyridine on the zinc porphyrin was parameterized with respect to the density functional distance and torsion scans. Based on the pre-optimized structures AM1 optimizations and frequency calculations are performed, followed by AM1* single point calculations.

Thermodynamic properties of the UHF AM1 frequency calculations were used to determine the Gibbs free energy of neutral, cationic and anionic optimized building blocks. The same was performed for the normal hydrogen reference electrode und the resulting values were used to determine the oxidation and reduction potentials. They are given versus Fc/Fc⁺ redox couple (0.4 V vs. NHE) to compare the calculated values with the experimental observed values.

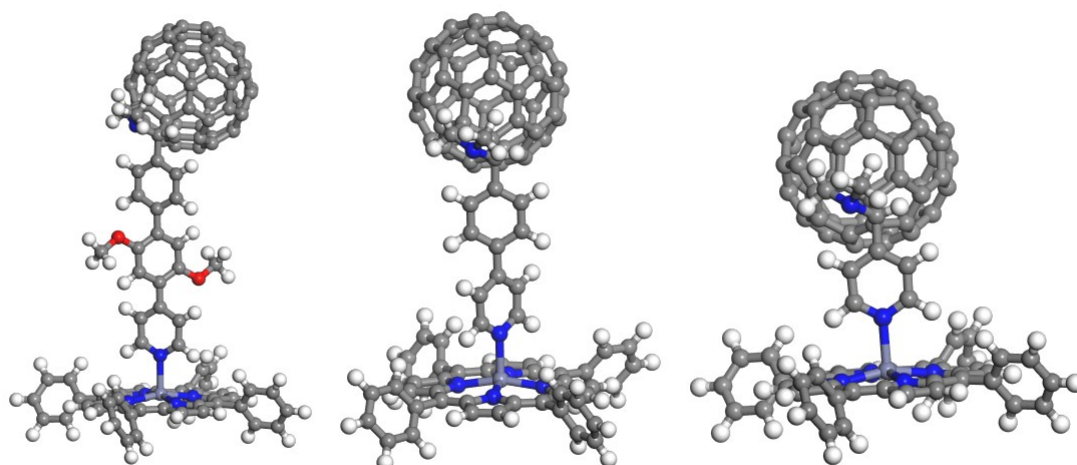


Figure S19 AM1 predicted structures for $C_{60}-(Ar)_2-Pyr \cdot ZnP$, $C_{60}-Ar-Pyr \cdot ZnP$ and $C_{60}-Pyr \cdot ZnP$.

	B3LYP/def2-TZVP D3BJ			AM1*	AM1* D3BJ
	gas phase	chlorobenzene	water	gasphase	gasphase
C₆₀-(Ar)₂-Pyr·ZnP	-20.44	-17.09	-15.85	-10.13	-21.20
C₆₀-Ar-Pyr·ZnP	-20.07	-16.76	-15.57	-10.04	-17.68
C₆₀-Pyr·ZnP	-29.42	-25.82	-24.56	-10.07	-21.69

Table S20 B3LYP/def2-TZVP and AM1* predicted dimerization energies for **C₆₀-(Ar)₂-Pyr·ZnP**, **C₆₀-Ar-Pyr·ZnP** and **C₆₀-Pyr·ZnP**.

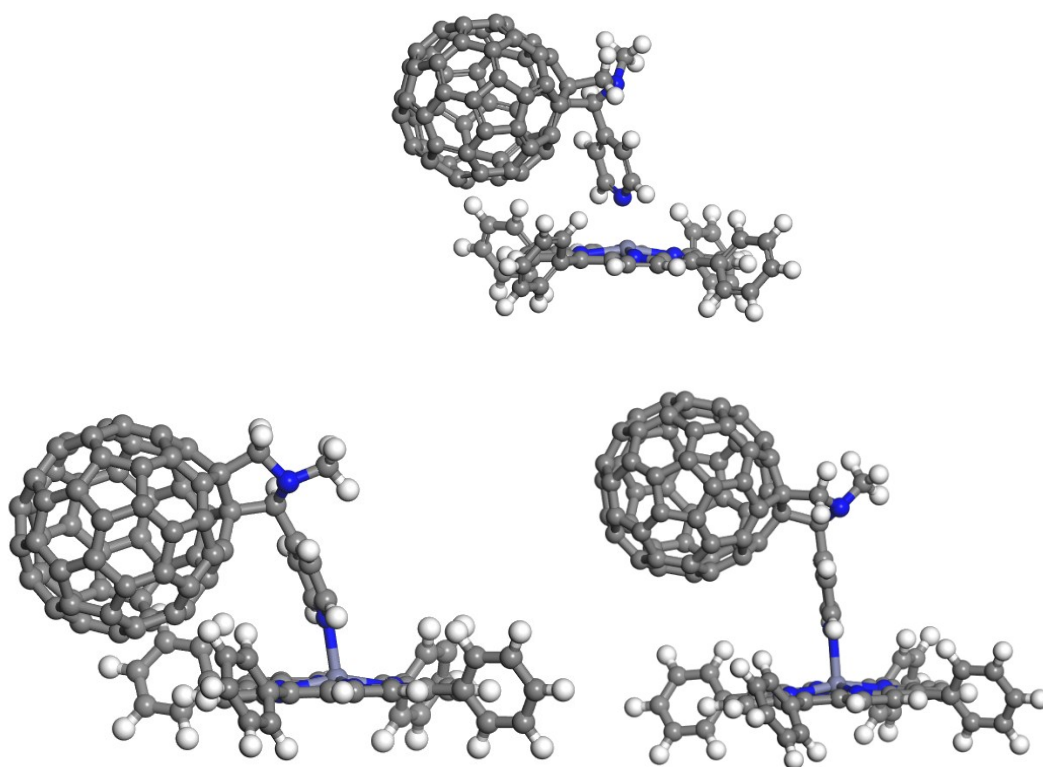


Figure S21 Structure comparison of C_{60} -Pyr·ZnP predicted with B3LYP/def2-TZVP including dispersion correction (left) and AM1 (right) and AM1 with D3BJ dispersion correction (bottom).

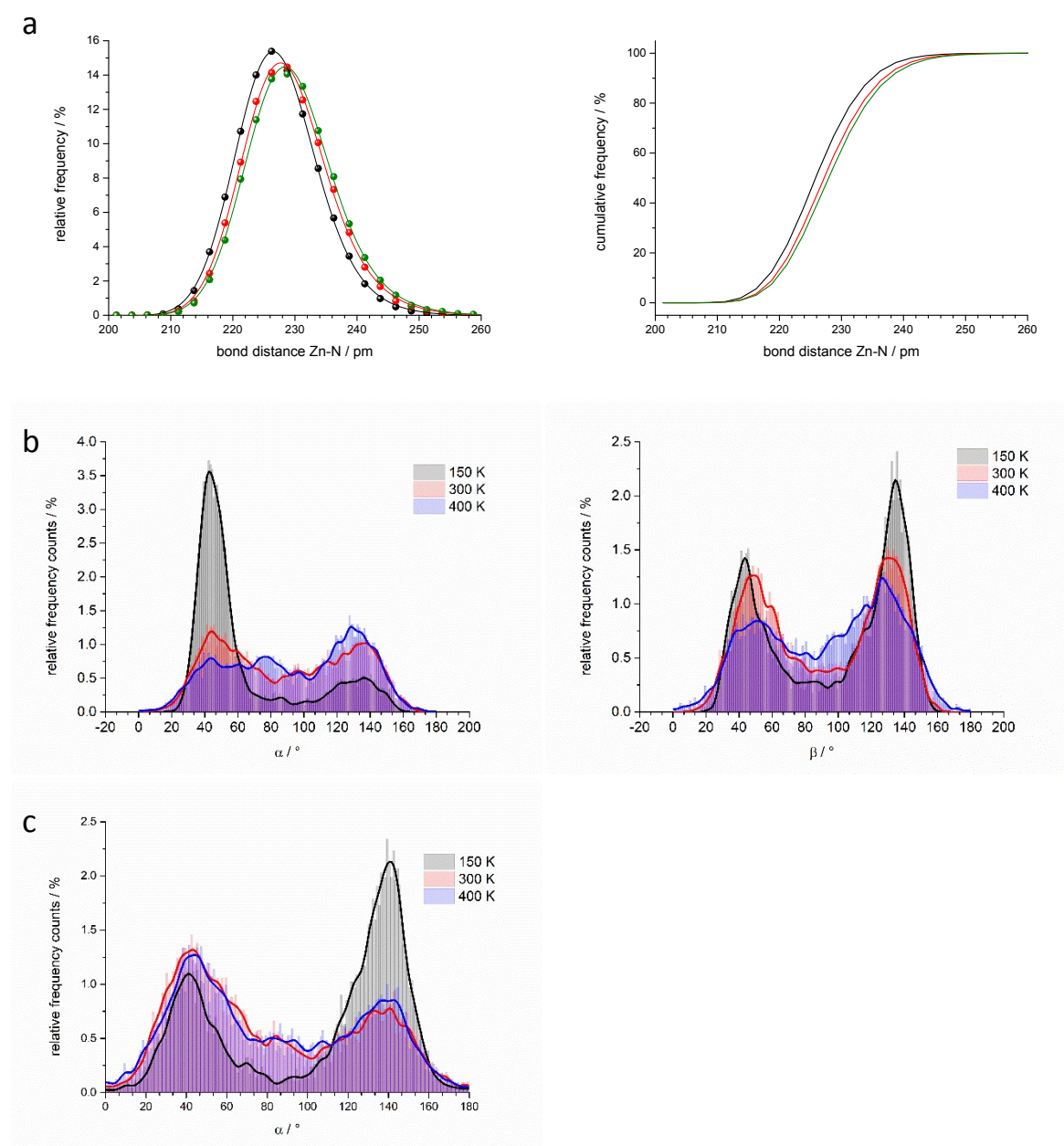


Figure S22 (a) Statistics on the length of the coordinating Zn-N bond during AM1 semiempirical MD calculations at room temperature (1ns duration, 0.5 fs time steps, snapshots every 50 fs). C_{60} -(Ar)₂-Pyr·ZnP (black) , C_{60} -Ar-Pyr·ZnP (red) and C_{60} -Pyr·ZnP (green) at 300K. (b) Statistic on dihedral

angle between pyridine and aryl group (left) and between neighboring aryl groups of the C_{60} -(Ar)₂-Pyr spacer during the MD simulation at different temperatures. (c) Statistic on dihedral angle between pyridine and aryl group (left) of the C_{60} -(Ar)-Pyr spacer during the MD simulation at different temperatures.

	compound	first oxidation / V vs Fc/Fc ⁺ ¹		
		theory	experiment	Deviation
bridge only	Benzene	1.44	1.48 ²	-0.04
	Biphenyl	1.07	1.09 ²	-0.02
	p-Diphenylbenzene	1.00		
	2,5-Diphenyl-1,4-dimethoxybenzene	0.70	0.80 ³	-0.10
	Pyridine	1.62		
	(Ar)-Pyr	1.37		
	4-(4-Biphenyl)pyridine	1.10		
	(Ar)₂-Pyr (out of plane)	0.78		
	(Ar)₂-Pyr (in plane)	0.79		
bridge + C ₆₀	Benzene	1.77		
	Biphenyl	1.08		
	p-Diphenylbenzene	1.01		
	2,5-Diphenyl-1,4-dimethoxybenzene	0.71		
	C₆₀-Pyr	1.86		
	C₆₀-(Ar)-Pyr	1.37	1.14 ⁴	0.23
	C ₆₀ -4-(4-Biphenyl)pyridine	1.11		
	C₆₀-(Ar)₂-Pyr (out of plane)	0.78	0.89 ⁴	-0.11
C₆₀-(Ar)₂-Pyr (in plane)	0.78	0.89 ⁴	-0.11	
	ZnTPP	0.24	0.21	0.03

	first reduction / V vs Fc/Fc ⁺		
	theory	experiment	deviation
C ₆₀	-1.28	-1.2	-0.08
Pyr	-2.14	-1.26	-0.02
Ar-Pyr	-1.75		
(Ar) ₂ -Pyr	-1.72		

Table S23 AM1 calculated oxidation and reduction potentials for various geometries.

¹ Fc/Fc⁺ reference was used to compare the results with the experimental values. Fc/Fc⁺ is set to 0.4 V vs NHE

2 Young-Kyu Han, Jaehoon Jung, Jeong-Ju Cho, Hyeong-Jin Kim, Chemical Physics Letters, Volume 368, Issues 5–6, 2003, Pages 601-608,
3 Noelia Fuentes, Luis Álvarez de Cienfuegos, Andrés Parra, Duane Choquesillo-Lazarte, Juan M. García-Ruiz, M. Luisa Marcos, Elena
Buñuel, Maria Ribagorda, M. Carmen Carreño, Diego J. Cárdenas and Juan M. Cuerva, Chem. Commun., Volume 47, Issue 5, 2011
4 this work

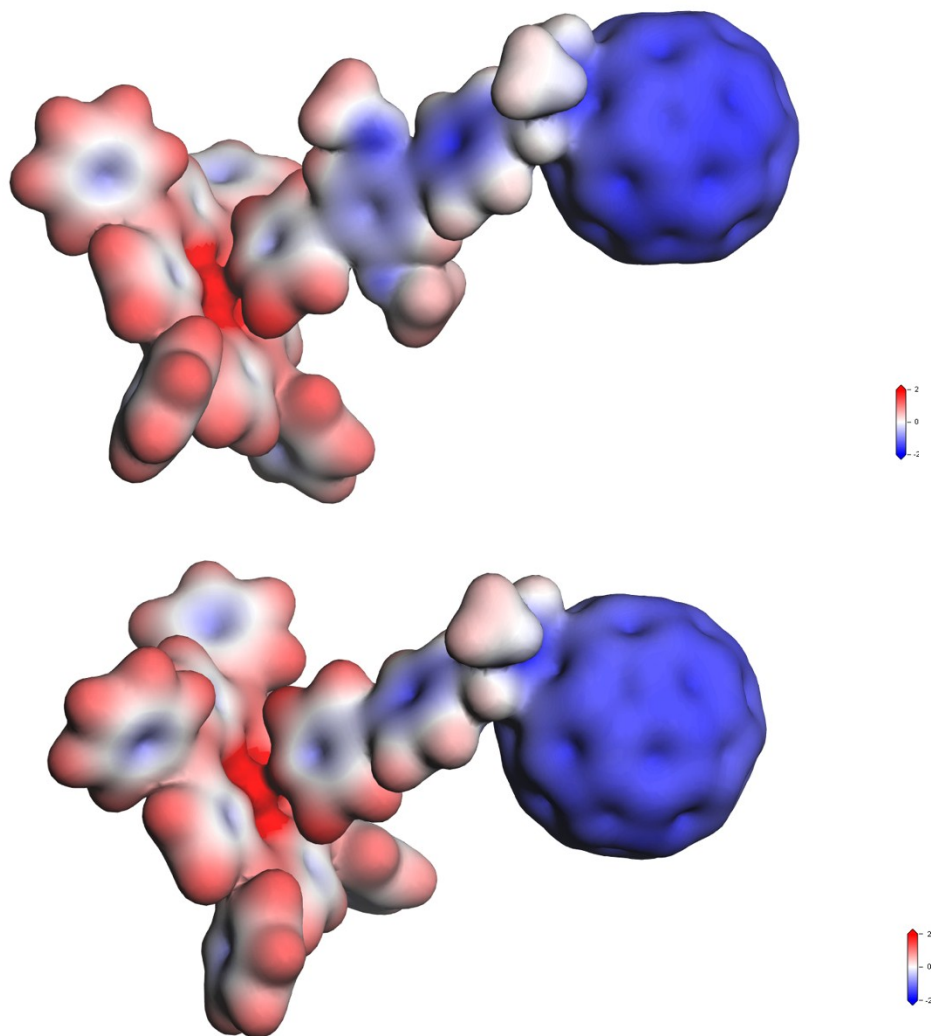


Figure S24 AM1 predicted charge transfer excited states for $C_{60}-(Ar)_2-Pyr \cdot ZnP$ (top) , $C_{60}-Ar-Pyr \cdot ZnP$ (bottom)

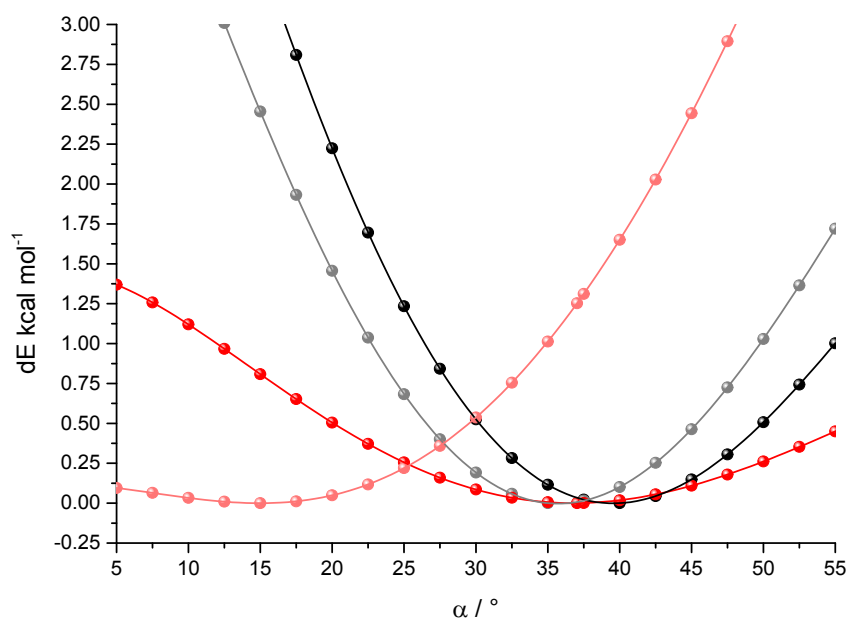
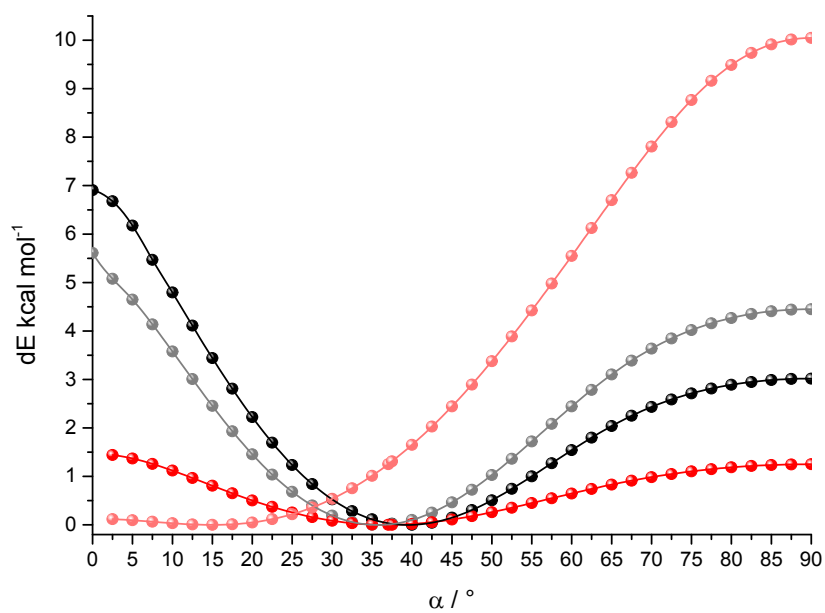


Figure S25 AM1 scan, varying the angle between neighboring phenyl rings, of $(Ar)_2$ -Pyr (black=neutral, grey=cation) and Ar-Pyr bridge (red=neutral, lightred=cation).

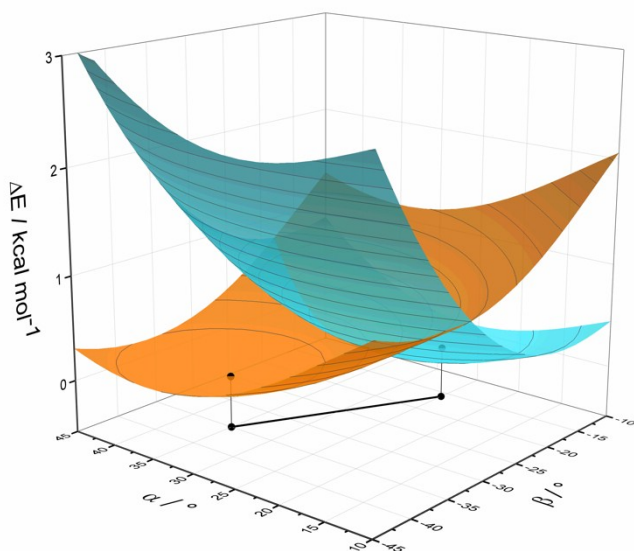
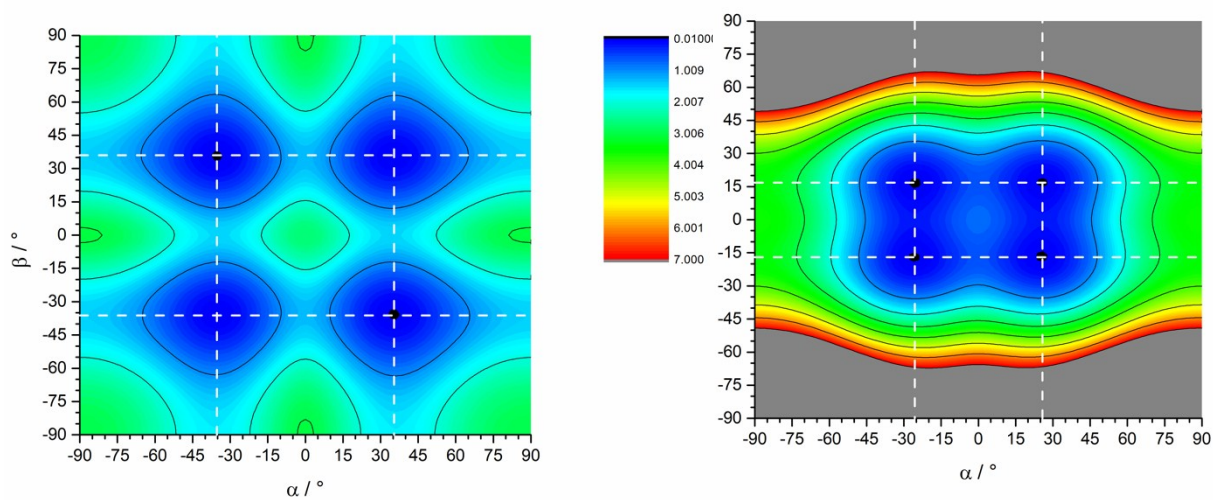


Figure S26 Top: AM1 UHF relaxed potential energy scan (energy difference from 0 to 7 kcal mol⁻¹, blue to red) of a 4-(4-Biphenyl)pyridine, rotating the torsion angles pyridine and phenyl (α) and between the neighboring phenyls (β). Left side shows the neutral groundstate singlet and right side the once oxidized cation doublet. **Bottom:** 3D representation of the potential energy surface for neutral singlet (orange) and cation doublet (blue).

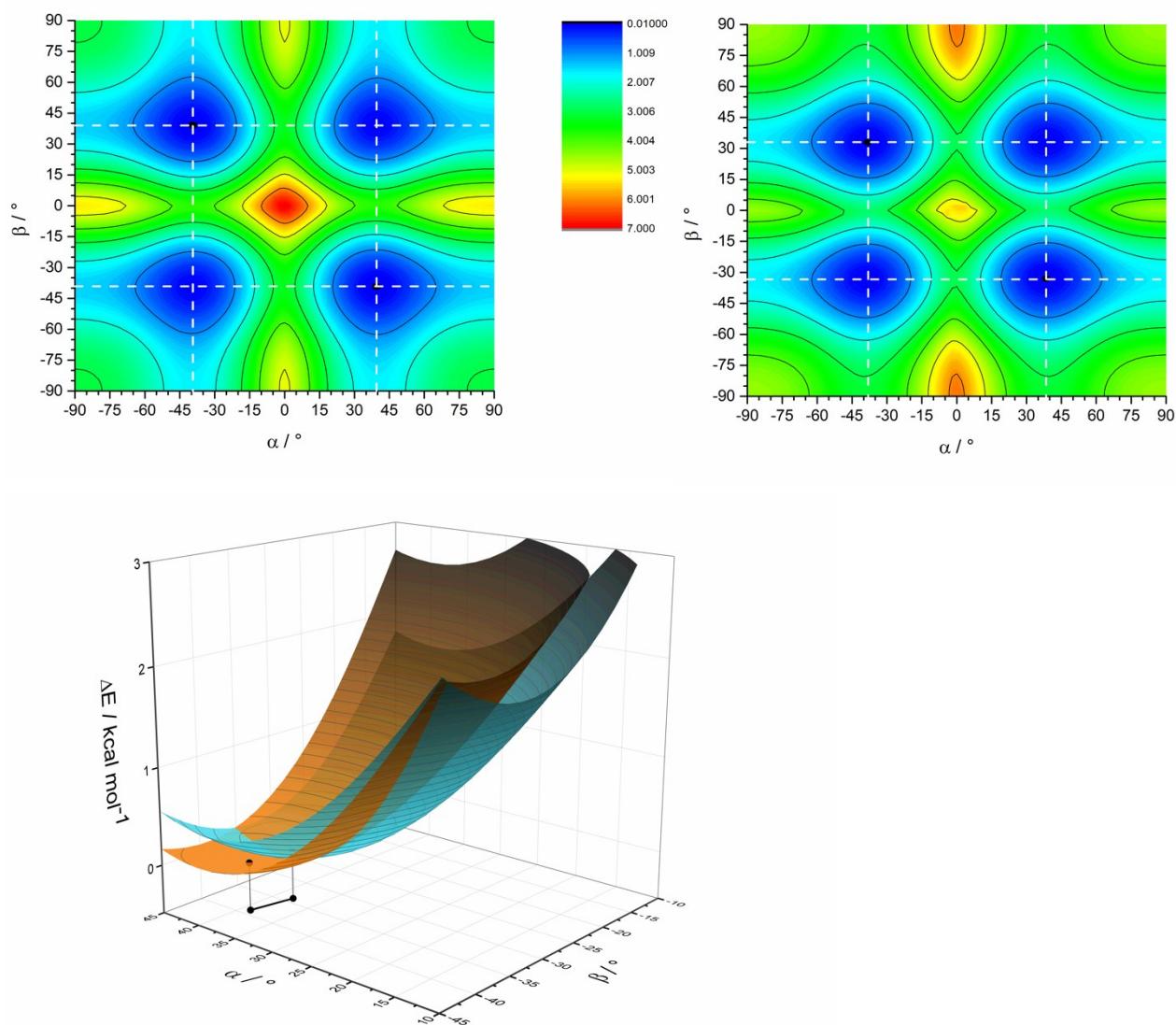


Figure S27 Top: AM1 UHF relaxed potential energy scan (energy difference from 0 to 7 kcal mol⁻¹, blue to red) of a **(Ar)₂-Pyr**, rotating the torsion angles pyridine and aryl (α) and between the neighboring aryl and phenyl (β). Left side shows the neutral groundstate singlet and right side the once oxidized cation doublet. **Bottom:** 3D representation of the potential energy surface for neutral singlet (orange) and cation doublet (blue).